From the Amelioration of a NADP+-dependent Formate Dehydrogenase to the Discovery of a New Enzyme: Round Trip from Theory to Practice

Heterogeneous & Homogeneous & Bio- & Nano-
CHEMCATCHEM
CATALYSIS

Accepted Article

Title: From the Amelioration of a NADP+-dependent Formate Dehydrogenase to the Discovery of a New Enzyme: Round Trip from Theory to Practice

Authors: Marina Simona Robescu, Rudy Rubini, Elisa Beneventi, Michele Tavanti, Chiara Lonigro, Francesca Zito, Francesco Filippini, Laura Cendron, and Elisabetta Bergantino

To be cited as: *ChemCatChem* 10.1002/cctc.201902089

Link to VoR: http://dx.doi.org/10.1002/cctc.201902089

A Journal of
ChemPubSoc Europe

WILEY-VCH www.chemcatchem.org

WILEY-VCH

FULL PAPER

From the Amelioration of a NADP+-dependent Formate Dehydrogenase to the Discovery of a New Enzyme: Round Trip from Theory to Practice

Marina Simona Robescu[+],[a] Rudy Rubini[+],[a] Elisa Beneventi,[a] Michele Tavanti,[a] Chiara Lonigro,[a,b] Francesca Zito,[b] Francesco Filippini,[a] Laura Cendron,*[a] and Elisabetta Bergantino*[a]

Abstract: NADP+-dependent formate dehydrogenases (FDHs) are biotechnologically relevant enzymes for cofactors regeneration in industrial processes employing redox biocatalysts. Their effective applicability is however hampered by the low cofactor and substrate affinities of the few enzymes described so far. After different efforts to ameliorate the previously studied *Gra*FDH from the acidobacterium *Granulicella mallensis* MP5ACTX8, an enzyme having double (NAD+ and NADP+) cofactor specificity, we started over our search with the advantage of hindsight. We identified and characterized *Gra*FDH2, a novel highly active FDH, which proved to be a good NAD+-dependent catalyst. A rational engineering approach permitted to switch its cofactor specificity, producing an enzyme variant that displays a 10-fold activity improvement over the wild-type enzyme with NADP+. Such variant resulted to be one of the best performing enzyme among the NADP+-dependent FDHs reported so far in terms of catalytic performance.

Introduction

Oxidoreductases are attractive biocatalysts for the synthesis of optically active compounds in chemical and pharmaceutical industries.[1,2] However, these industrially relevant enzymes are cofactor-dependent, as they require a reduced nicotinamide NAD(P)H cofactor for the catalysis.[3] The high cost of NAD(P)H prevents its stoichiometric supply, therefore an effective cofactor regeneration system is needed in industrial-scale applications.[4,5] Nicotinamide regeneration enzymes generally used in commercial processes (as second enzymes in combination with a second regeneration substrate) are glucose dehydrogenases (GDHs) and formate dehydrogenases (FDHs); few examples are reported for alcohol dehydrogenases (ADHs), whereas phosphite dehydrogenases (PDHs) have just been tested at the laboratory scale.[5]

[a] Dr. M. S. Robescu, R. Rubini, Dr. E. Beneventi, Dr. M. Tavanti, C. Lonigro, Prof. F. Filippini, Dr. L. Cendron, Prof. E. Bergantino
Synthetic Biology and Biotechnology Unit, Department of Biology, University of Padova
via U. Bassi 58B / viale G. Colombo 3, I-35131 Padova, Italy
*E-mail: laura.cendron@unipd.it; elisabetta.bergantino@unipd.it

[b] C. Lonigro, Dr. F. Zito
Laboratoire de Biologie Physico-Chimique des Protéines Membranaires, UMR7099, CNRS, IBPC, Université Paris Diderot, Sorbonne Paris Cité
13 rue Pierre et Marie Curie, 75005, Paris, France.

[+] *These two authors contributed equally to this work.*

Supporting information for this article is given via a link at the end of the document.

NAD(P)+-dependent FDHs (EC 1.17.1.9) catalyze the oxidation of formate into carbon dioxide, coupled with the reduction of the cofactor NAD(P)+ to NAD(P)H. FDHs are reasonable candidates for regenerating NAD(P)H since they have several advantages over any alternative enzyme. First, the reaction they catalyze is irreversible and the gaseous nature of the CO_2 product provides thermodynamic pressure by leaving the mixture, shifting the equilibrium to the formation of the desired product in the coupled reaction. This also facilitates the separation of the products and so the downstream processing. Moreover, the sacrificial substrate, formate, is a cheap, stable and soluble compound. Together with their low cost of production and wide pH optimum (6.0 – 9.0), FDHs could potentially have many useful biocatalytic applications.[6,7] However, most known such enzymes are NAD+-dependent and, at least to date, only a few native NADP+-dependent FDHs have been identified.[6,8–13] This is a major drawback, as NADPH is widely used as cofactor in industrial bio-transformations and it is much more expensive than NADH.[4]

A number of engineering efforts focused on the modification of known FDHs to switch their cofactor preference towards NADP+. NAD+-dependent FDHs are endowed with a conserved NAD+ binding motif G(A)XGXXG(X)$_{17\text{-}18}$D(E), where X is any amino acid and the negatively charged C-terminal aspartate (or glutamate) can interact with the 2'- and 3'-OH of NAD+ ribose ring, repelling the additional phosphate of NADP+.[14,15] In engineering studies, the conserved aspartic/glutamic acid responsible for the NAD+ preference has thus to be replaced by a neutral or cationic amino acid. This is confirmed by the reverse cofactor specificity shift (from NADP+ to NAD+) that could be obtained in *Bst*FDH (from *Burkholderia stabilis*) by site specific single mutation (Q223D).[10]

The first engineered enzyme specific for NADP+, *Pse*FDH (from *Pseudomonas sp*. 101), was obtained in 1993 but no details about amino acid substitutions have been described,[16] while a single mutation (D195S, corresponding to Q223 in *Bst*FDH) in *Candida methylica* FDH was sufficient to shift its cofactor specificity towards NADP+.[17] More recently, further variants were obtained from *Candida boidinii* FDH by structure guided site saturation mutagenesis of residues D195, Y196 and Q197; this allowed the identification of double (D195S/Q197T and D195S/Y196L) and triple (D195Q/Y196R/Q197N) mutations able to increase the catalytic efficiency with NADP+.[18,19] The FDH from *Mycobacterium vaccae* N10 was also engineered to modify cofactor specificity and to increase the chemical stability of the enzyme. The most promising variants harbored the double mutations A198G/D221Q and others, in which the synergistic effect of the substitutions of C145 and C255 were investigated.[15] Finally, the role of A198 (*Pse*FDH numbering), that has "forbidden" values of the φ and ψ angles in many solved bacterial FDH structures was analyzed in deepth.[20] A198 in NADP+-dependent

enzymes was suggested to provide efficient formate binding and to improve binding of $NADP^+$ itself.[15] Nevertheless, to our knowledge, none of aforementioned efforts could successfully address the industrial application of any $NADP^+$-dependent FDH. A closer examination of these studies shows that in many instances, cofactor specificity change was marginally achieved and resulted in a compromised catalytic activity.[21]

We have previously isolated a FDH from the acidobacterium *Granulicella mallensis* MP5ACTX8 (*Gra*FDH) accepting both cofactors and showed the role of A222 (corresponding to Q223 in *Bst*FDH) in determining its peculiar dual specificity. Since that enzyme displayed good resistance to common organic solvents and tolerance to acidic conditions, it was considered a potential candidate for the biocatalytic regeneration of NADPH, provided an amelioration of its catalytic performance.[6] Different approaches of rational design or directed evolution failed in producing enzyme variants with boosted k_{cat}. We then changed our strategy and opted for switching the cofactor preference of an already well performing enzyme rather than trying to improve the kinetic parameters of a weak biocatalyst. Indeed, the rational engineering of the newly identified NAD^+-dependent *Gra*FDH2 was successful in changing its specificity towards $NADP^+$ and achieving one of the best performing $NADP^+$-dependent FDH reported so far.

Results and Discussion

Improvement of *Gra*FDH enzymatic performances

Among the few known native $NADP^+$-dependent FDHs, the previously characterized *Gra*FDH showed double cofactor specificity together with good stability at low pH and in organic solvents; however, its low affinity for both the substrate and the cofactors deterred employment in biocatalysis. Indeed, the necessity of an improvement in its enzymatic performance was clear since the original publication.[6]

To the aim of ameliorating *Gra*FDH, we planned both rational design and directed evolution. In the former approach, several point mutations based on the exam of its crystallographic structure were designed to improve its catalytic efficiency (Table S1 and Supporting Information for details). Briefly, it was possible to purify only few variants, the other ones being insoluble in *E. coli*. Among the characterized variants, only the mutations A222Q and K380H where shown to increase the preference for $NADP^+$ over NAD^+ while not improving efficiency (Table S1).

This prompted us to shift to a directed evolution approach and we designed an innovative and smart *in vivo* strategy: it was based on the expression of an active *Gra*FDH in the chloroplast of the unicellular green alga *Chlamydomonas reinhardtii*. The rationale for selection was the following: formate anions inhibit photosynthesis by precisely affecting Photosystem II[22] and thus the expression of an active FDH into the chloroplast should allow formate conversion into CO_2 leading to formate-resistant, CO_2-consuming cells with restoration of photosynthesis. As a result, highest autotrophic growth in presence of formate would correspond to the cells expressing the most efficient variants of FDH.

An expression library (Figure S1) engineered to express randomly mutated variants of *Gra*FDH into the chloroplast was used to transform *C. rehinardtii* by the biolistic method. Six selected *Gra*FDH variants once again faced solubility problems upon expression in *E.coli*: despite numerous attempts adopting different expression strategies, only two variants (Figure S2) could be partially purified and a single one could be examined. Its k_{cat} in the reaction with $NADP^+$ was not improved with respect to the *wild-type Gra*FDH, while its activity with NAD^+ was completely abolished (Table S2) (for more details about this work package, see Supporting Information). Failure of this second attempt convinced us to reconsider the overall strategy by start searching for eventual novel FDH enzyme(s) in *G. mallensis* (thus keeping the same molecular adaptations of an extremophile enzyme as *Gra*FDH) with better catalytic features. To this aim, we left search settings open to the most common NAD^+-dependent FDHs, with the aim to shift then preference for the cofactor towards $NADP^+$.

In silico identification and analysis of a novel putative FDH: *Gra*FDH2

We used the *Gra*FDH wild-type sequence as a probe for homology search in the *G. mallensis* MP5ACTX8 proteome and identified a putative paralog (AEU35217.1), hereafter called *Gra*FDH2. Reciprocal blast hit search demonstrated that *Gra*FDH and *Gra*FDH2 are the only two FDHs encoded by the *G. mallensis* genome. Sequence comparison shows high identity between the two proteins (id: 76 %, pos: 86 %), probably derived by an early duplication of a common ancestor, and suggests *Gra*FDH2 is endowed with NAD^+ specificity. Indeed, the alignment in Figure S3 highlights residues crucial for cofactor specificity, which are A222 in *Gra*FDH and D222 in *Gra*FDH2, being aspartate the most reported residue at this position in NAD^+ specific FDHs.[14] It is noteworthy that the two FDHs also differ in neighboring residue 223 (R in *Gra*FDH and Q in *Gra*FDH2). In particular, in $NADP^+$ specific proteins, R223 interacts through H-bonds with the phosphomonoester group.[6]

The high sequence identity between the two paralogs allowed obtaining a reliable structural model of *Gra*FDH2 target using *Gra*FDH structure (4XYG) as template via Homology Modelling. After model refinement and model quality assessment, we determined the spatial distribution of the electrostatic potential for both paralogs, focusing on the role of surface charge distribution as visualized by isopotential contours. This highlighted relevant differences in the substrate channel; then, with the availability of the crystallographic structure (see forward), the actual electrostatic map confirmed such differences (Figure S4) that resulted even more pronounced than in the modelled structure.
As shown by close up views in Figure 1 the density of negative potential (red) at the catalytic cavity entry is higher for *Gra*FDH, with positive (blue) or neutral (white) potential at the same positions for *Gra*FDH2. *Gra*FDH has additional negatively charged residues at positions 263 and 287 (E263, E287), forming a negative cluster (together with D290 and D293). This could explain the low affinity of *Gra*FDH for the formate anion and is

suggestive for higher affinity of the less negative cavity of *Gra*FDH2, which has a neutral non-polar residue (L263) and two opposite positive charges (K287, K318) attracting the anionic substrate. A number of additional negative charges (E80, D81 and E131) is likely to favor by repulsion the interaction of substrate molecules with the aforementioned positively charged track in the binding cleft of the novel enzyme. These peculiar features prompted us to express and characterize *Gra*FDH2.

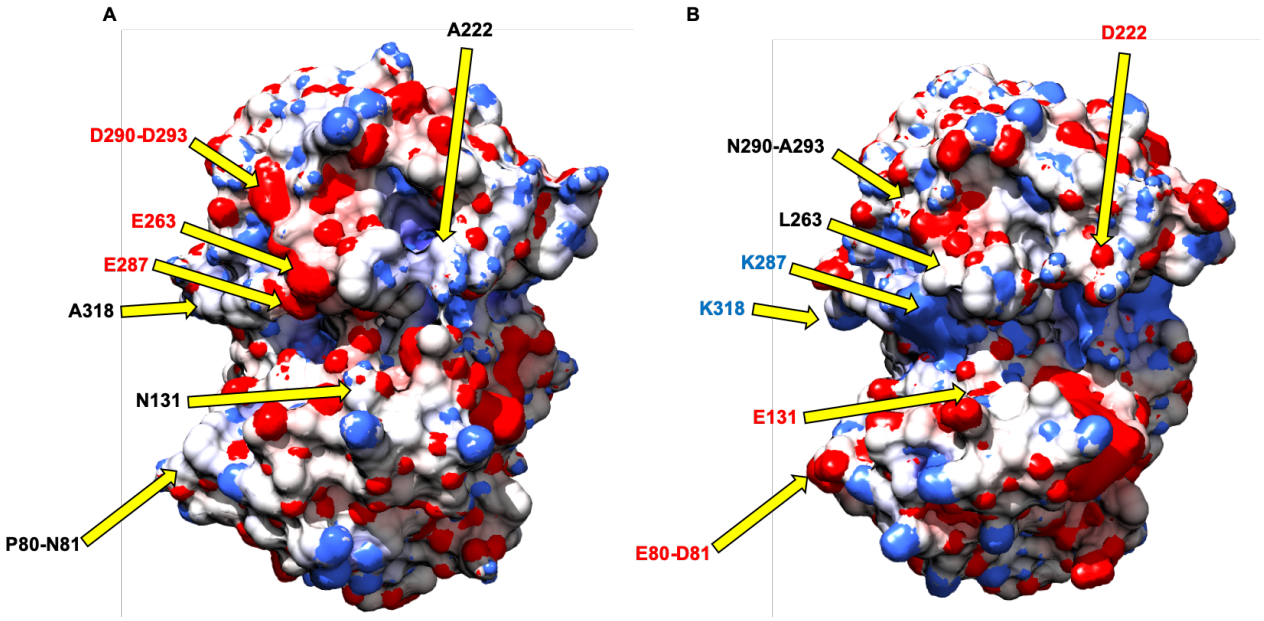

Figure 1. Comparative analysis of surface charge distribution. It is visualized by isopotential contours at I = 100 mM and pH 7.5. *Gra*FDH (apo) structure (pdb 4XYG) is on the left (**A**), *Gra*FDH2 apo structure (pdb 6T8C) on the right (**B**). Density of negative potential is red, positive is blue and neutral is white. Focusing on *Gra*FDHs catalytic cavities, yellow arrows highlight the main differences in the cavity entry, while amino acid one-letter codes and residue numbers are reported in black, blue or red for neutral, positively charged or negatively charged residues, respectively.

Expression and characterization of the novel *Gra*FDH2

The *Gra*FDH2 coding sequence was expressed in *E. coli* cells in fusion to a C-terminal His_6-tag. The protein was then purified in soluble form at high yield (76 mg per liter of culture). SDS-PAGE analysis (Figure 2A) showed a pure and homogeneous protein band with electrophoretic mobility corresponding to the calculated molecular mass of the monomer (43 kDa). The estimated molecular weight of *Gra*FDH2 from analytical Size Exclusion Chromatography (SEC) experiment is 1.55 times that of the monomeric species, suggesting dimer formation (Figure 2B).

Initially, the activity of *Gra*FDH2 as formate dehydrogenase was demonstrated *in vitro* with different concentrations of both nicotinamide cofactors (Table 1). As expected, it showed preference for NAD^+ as cofactor like the majority of known FDHs[23] (up to 5.28 ± 0.14 U mg^{-1}), with very low activity in presence of $NADP^+$ (0.34 ± 0.11 U mg^{-1}). In comparison to *Gra*FDH, *Gra*FDH2 showed a 4.5-fold higher biocatalytic efficiency for formate in presence of NAD^+ (K_M 10.51 ± 1.62 mM, k_{cat} 3.84 ± 0.11 s^{-1}) and, as expected, better kinetic constants for NAD^+ (K_M 0.22 ± 0.01 mM, k_{cat} 3.78 ± 0.05 s^{-1}). The kinetic characterization highlighted the better performances of *Gra*FDH2; in particular, its 10-fold lower K_M value for formate is very similar to the best reported recombinant FDHs,[24] whose K_M values range between 3 and 10 mM while those for NAD^+ range between 0.03 and 1.20 mM.[23,24]

As expected, *i.e.* similar to its paralog, *Gra*FDH2 showed initial activity in a broad range (4.0-12.0) of pH (Figure 2C) with the highest specific activity (5.06 ± 0.11 U mg^{-1}) at pH 5.0, matching the physiological values for *G. mallensis* growth (pH 3.5 - 6.5),[25] significantly decreasing only at pH 4.0. This can be considered as a positive feature for a biocatalyst, since it may be capable of regenerating the reduced coenzyme in reactions with different condition demands.

Thermofluor analysis revealed a favorable thermostability (T_m of 64 °C) when compared to *Gra*FDH (57 °C).[6] The T_m is the same at pH 7.0 and 9.0, decreasing only below the theoretical pI, at pH 5.0 (56 °C). The enzyme also exhibited good tolerance in the presence of 5 % to 10 % methanol, ethanol, isopropanol and DMSO, while decreased stability was observed with 10% *tert*-butanol or higher concentrations of this co-solvent. The highest concentrations (40 %) of ethanol, methanol and DMSO had a detrimental effect on protein stability, decreasing the T_m by 20 to 15 °C. In the higher percentage of isopropanol and *tert*-butanol the protein was completely denatured (Figure 2D).

Although estimated with different methods, a brief comparison with the thermostability of other FDHs can be made. Indeed, the apparent melting temperature measured for *Gra*FDH2 falls in the

upper range of values reported in the literature (57.9 and 64.5 °C). The most thermostable enzymes described are the ones from *Pseudomnas sp*. 101 (67.6 °C)[26] and from *Lactobacillus buchneri* (78 °C).[8]

Once demonstrated the better biocatalytic performance of *Gra*FDH2, we moved to the second step in strategy, *i.e.* changing its cofactor specificity. In order to properly feed rational engineering by a real structure rather than a model, we decided to solve the three-dimensional structure of *Gra*FDH2 by X-ray crystallography.

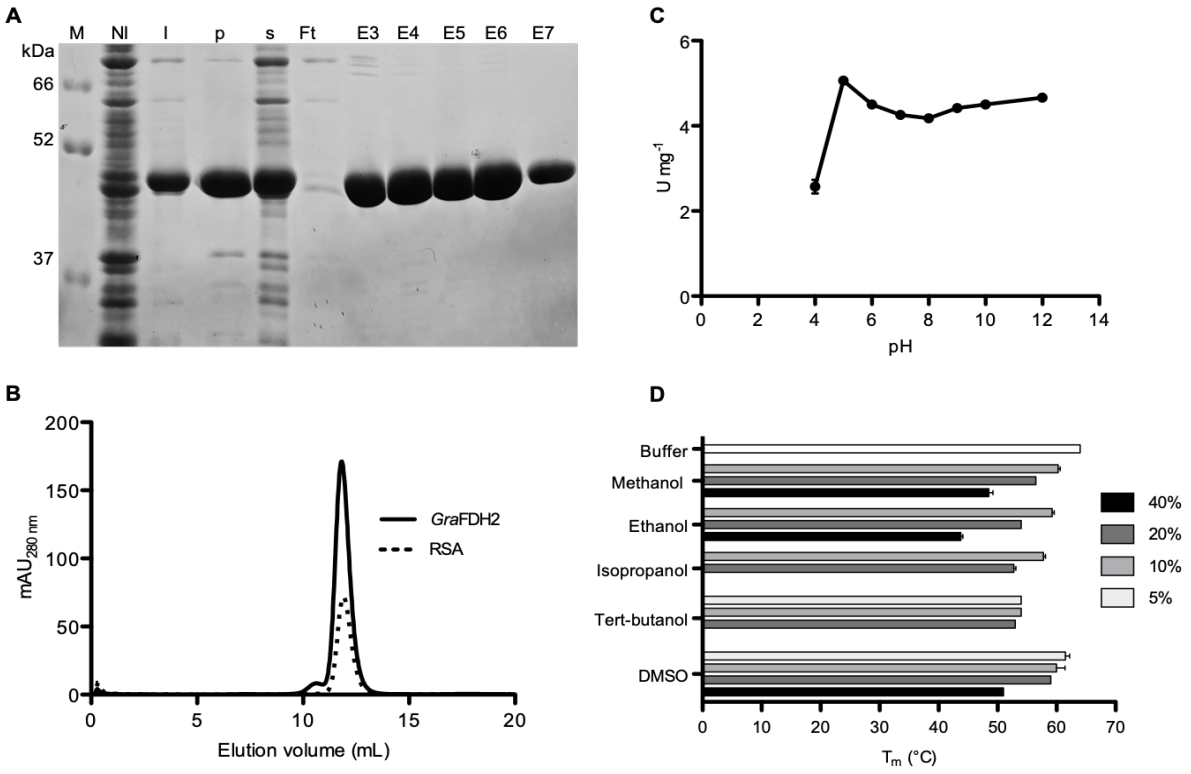

Figure 2. Production and biochemical characterization of the wt GraFDH2 enzyme. (**A**) 12 % SDS-PAGE analysis of cell extracts from *E. coli* BL21 cells expressing *Gra*FDH2: Prestained Protein SharpMassTM VII protein ladder (M), total cell extracts from non induced cells (NI) and over-night induced cells (ON), pellet fraction (p), soluble protein fractions (s), flow through (Ft), IMAC eluted fractions (E). (**B**) Analytical size exclusion chromatography samples eluted from a Superose 12 10/300 GL column. (**C**) *Gra*FDH2 activity-pH profile. The specific activity (U mg^{-1}) of the enzyme was determined using a universal buffer of constant ionic strength: Tris-HCl (0.1 M), MES (0.05 M), and CH_3COOH (0.05 M) adjusted to the different pH values (4.0, 5.0, 6.0, 7.0, 8.0, 9.0, 10.0, 11.0 and 12.0) at 25 °C by using NaOH (5 M) or HCl (5 M). (**D**) Influence of type and concentration of co-solvents (KH_2PO_4 buffer (pH 7.5, 0.1 M) supplemented with increasing vol % of organic co-solvent) on *Gra*FDH2 T_m.

Deep structural analysis and rational engineering of the cofactor binding site

*Gra*FDH2 crystal structure - determined either in the apo form (pdb 6T8C) or in complex with NAD^+ cofactor and azide (NaN_3) inhibitor (pdb 6T8J) (Table S4) - shows the typical dimeric fold of bacterial formate dehydrogenases,[23] as inferred from SEC analysis (see Supporting Information for deeper details).

Both NAD^+ molecule and azide ion are clearly visible in the electron-density map of holo *Gra*FDH2. Azide ion occupies the same binding site as formate ion above the nicotinamide ring, mimicking the transition state of the enzymatic reaction, according to the proposed mechanism of FDHs.[27] In the catalytic site of holo *Gra*FDH2, azide ion is bound to residues belonging to both the coenzyme-binding domain (R285 and H333) and the catalytic domain (I123 and N147) (Figure 3A). Interestingly, the catalytic residue H333 establishes a direct hydrogen bond with the azide ion as reported also for *Mor*FHD[28] but not for *Pse*FDH[29] where the distance between the target atoms is about 3.6 Å. Moreover, in the holo form residues R285 and D126 flip their orientation and act as a wall in closing the substrate channel entrance.

The NAD^+ cofactor interacts mainly with residues of the coenzyme-binding domain (Figure S5), very well conserved in all FDHs. The cofactor binding causes conformational changes of the residues in the binding region of the adenine moiety of the cofactor. In this region, deviations of carbon α atoms > 1.5 Å are observed for residues 122-124, 221–226 and 255–275. As observed with *Gra*FDH and *Pse*FDH, this conformational switch leads to a more compact and closed active site pocket. However,

the observed rearrangement of the two globular domains is not as dramatic as reported for other FDHs.[29,30] Indeed, the superposition of the apo and holo structure of *Gra*FDH2 has an r.m.s.d. over Cα atoms of 0.8 Å (Gesamt software)[31] with deviations over 1.5 Å, observed in the binding region of adenine moiety of the cofactor (residues D222-H225), and the region between residues A256-I271. Therefore, *Gra*FDH2 seems to have a more rigid structure with a closed conformation of the inter-domain cleft also in the apo form, as already reported for *Mor*FDH.[28] Moreover, when compared to *Gra*FDH and *Pse*FDH, the C-terminus of the holo *Gra*FDH2 maintains a more flexible nature, making it almost untraceable in the electron-density maps after A375. The terminal residues stretch, from G371 to A375, assumes two different conformations according to the local environment mainly dictated by crystals contacts experienced by the different copies in the asymmetric unit. In FDHs, the C-terminal fragment is known to get structured in the holo form and to be directly involved into cofactor interactions.[28]

As shown in the close-up view in Figure 3D, an extra phosphate group attached to the O29 of the NAD-ribose (as in $NADP^+$) would collide with the side chains of D222, Q223 and H224, thus causing steric clashes. This aspartic residue (D222 in *Gra*FDH2), is highly conserved between the NAD^+ specific FDHs being a major determinant of specificity for NAD^+. In the naturally $NADP^+$ specific FDHs it is replaced by either glutamine (*Bst*FDH[10] Q223), alanine (*Gra*FDH[6] A222) or serine (*Bd*FDH[12] S223).

In order to change *Gra*FDH2 cofactor specificity, we focused engineering at the relevant positions 222 and 223. Five different D222X/Q223X double mutantions were designed based on comparative sequence and structural analysis of a number of representative catalytic sites. Mutant D222A/Q223R has the corresponding residues that are present in *Gra*FDH, and its reciprocal mutant D222R/Q223A allowed to investigate the effects of a positive charge at position 222. Mutant D222Q/Q223R was inspired by other two native $NADP^+$-dependent FDH (*Bst*FDH and *Lb*FDH), with the additional alternative D222N/Q223R, replacing glutamine by the chemically equivalent asparagine, with a reduced steric hindrance. Finally, mutant D222S/Q223R was designed based on previous attempts on multiple FDHs and inspired by *Bd*FDH, a native $NADP^+$-dependent FDH.[17,33]

Production and characterization of the designed *Gra*FDH2 variants

Recombinant expression of the engineered proteins was performed as for the wt enzyme. We first investigated the solubility of the five *Gra*FDH2 mutant proteins. Four of them showed an acceptable solubility, even if lower than their wt counterpart (Figure S6). D222R/Q223A was excluded from further purification and characterization steps due to its low solubility. The purification yield of the mutant proteins resulted between 15 and 20 mg per liter of culture in all cases. Thermal shift experiments revealed melting temperature values very similar to the wt enzyme for all characterized variants, that therefore maintained the same thermal and co-solvent stability (Figure S7).

Activity tests confirmed that all four enzyme variants had improved cofactor specificity towards $NADP^+$. Specific activities of *Gra*FDH2 wt and variants, at different concentrations of $NAD(P)^+$, are listed in Table 1.

Table 1. Specific activity of *Gra*FDH2 wt and variants in standard assay conditions.[a]

Enzyme	U mg^{-1} (NAD^+)	U mg^{-1} ($NADP^+$)
*Gra*FDH2 wt	5.28 ± 0.14[b] 5.09 ± 0.04[c]	0.34 ± 0.11[b] 0.14 ± 0.02[c]
D222N/Q223R	3.02 ± 0.04[b] 3.01 ± 0.11[c]	1.88 ± 0.02[b] 1.70 ± 0.01[c]
D222Q/Q223R	2.20 ± 0.25[b] 1.74 ± 0.14[c]	1.96 ± 0.09[b] 1.96 ± 0.04[c]
D222A/Q223R	3.14 ± 0.11[b] 2.75 ± 0.02[c]	2.70 ± 0.09[b] 2.48 ± 0.09[c]
D222S/Q223R	2.97 ± 0.14[b] 2.74 ± 0.05[c]	3.20 ± 0.18[b] 2.84 ± 0.18[c]

[a] The standard assay was performed at 25° C using sodium formate (0.1 M) and $NAD(P)^+$ cofactor (0.02 M[b] or 0.005 M[c]). Enzyme concentration was 30 μg mL^{-1} in KH_2PO_4 buffer (pH 7.5, 0.1 M).

After that, also their kinetic parameters were determined, as reported in Table 2.

The best variant was found to be D222S/Q223R, showing a 10-fold activity improvement over the wt enzyme in presence of $NADP^+$. Intriguingly, the affinity for formate was almost identical to the wt (11.57 ± 1.09 mM) with NAD^+ and, importantly, remained very good (23.66 ± 1.58 mM) even with $NADP^+$. Amazingly, the latter K_M value is one of the lowest among $NADP^+$-dependent FDHs reported so far (Table 3), the latter showing values from 5.66 to 200 mM. D222S/Q223R variant shows the third best biocatalytic efficiency for formate in presence of $NADP^+$ (1.49×10^2 M^{-1} s^{-1}) among known FDHs. The kinetic parameters for both cofactors confirmed that the enzyme has acquired a preference for $NADP^+$, with good affinity and biocatalytic efficiency values of 0.136 ± 0.016 mM and 2.26×10^4 M^{-1} s^{-1}, respectively.

The other three variants displayed the desired shift towards $NADP^+$ as well, with Michaelis constant values between 0.144 and 0.516 mM. However, the affinity towards the substrate was limited, with K_M values ranging from 62.46 to 161.00 mM. This effect on formate binding might depend on structure alterations caused by the introduced mutations. In order to gain insights into catalytic properties between the different enzyme variants, we proceeded with their structural characterization.

Table 2. Comparison between kinetic parameters of *Gra*FDH and of the engineered *Gra*FDH2 variants.

Enzyme	k_{cat} formate (s^{-1})	K_M formate (mM)	k_{cat} / K_M (M^{-1} s^{-1})	k_{cat} NADP+ (s^{-1})	K_M NADP+ (mM)	k_{cat} / K_M (M^{-1} s^{-1})
*Gra*FDH wt[a]	6.11 ± 0.24	191.25 ± 18.82	3.19 x 10^1	3.96 ± 0.27	0.850 ± 0.149	4.66 x 10^3
D222N/Q223R	2.14 ± 0.05	62.46 ± 5.03	3.43 x 10^1	2.08 ± 0.05	0.516 ± 0.061	4.03 x 10^3
D222Q/Q223R	3.18 ± 0.12	161.00 ± 20.97	1.97 x 10^1	2.46 ± 0.06	0.114 ± 0.015	2.16 x 10^4
D222A/Q223R	4.29 ± 0.08	86.10 ± 6.30	4.98 x 10^1	3.83 ± 0.07	0.215 ± 0.019	1.78 x 10^3
D222S/Q223R	3.53 ± 0.06 (3.07 ± 0.07)[b]	23.66 ± 1.58 (11.57 ± 1.09)	1.49 x 10^2 (2.65 x 10^2)[b]	3.08 ± 0.06 (3.49 ± 0.05)[b]	0.136 ± 0.016 (0.764 ± 0.041)[b]	2.26 x 10^4 (4.57 x 10^3)[b]

[a]*Gra*FDH data from our previous work.[6] Standard assay (100 µl) performed at 25° C in KH_2PO_4 (pH 7.5, 0.1 M), 30 µg mL^{-1} FDH enzyme. Parameters for the substrate were determined with $NADP^+$(0.005 M) or with NAD^+ (0.005 M)[b]. Nicotinamide cofactors kinetics were investigated with sodium formate (0.5 M), except for D222S/Q223R for which 0.2 M sodium formate was used with both cofactors.

*Gra*FDH2-D222X/Q223X X-ray crystal structure

The crystal structure of the mutant proteins D222S/Q223R, D222A/Q223R and D222Q/Q223R have been determined in complex with $NADP^+$ and sodium azide with very similar data quality and resolutions close to 2 Å (Table S5). Overall structures well superpose as expected, with minimal main chain r.m.s.d. in the case of D222S/Q223R (0.032 Å) and slightly higher in the case of D222A/Q223R and D222Q/Q223R (0.504 and 0.512 Å respectively). Different crystal packing as well as peculiar features due to crystallization conditions have been encountered and carefully taken into account during structural comparison.

In particular, the D222S/Q223R mutant crystallized using a precipitant agent including a mixture of divalent cations. As a consequence, a clear electron density coordinated at the entrance of the active site, in close proximity to the mutated loop and $NADP^+$ cofactor, has been detected in both Furier difference and anomalous maps and thus attributed to cobalt ions. At least two metal ions are bound at the mouth of the active site, the first involving H224 in its coordination sphere and other unknown ions, possibly including water molecules, the second trapped between H259 side chain and $NADP^+$ phosphate (see Supporting information, Figure S8).

The conformational changes that occur upon cofactor binding, clearly visible in the structures of apo and holo forms of the *Gra*FDH2 wt enzyme (Figure 3A and 3B), are here conserved, with all the variants loaded with $NADP^+$ and azide assuming such a closed and more compact conformation. Peculiar of the D222A/Q223R mutant protein is the presence of one out of the four molecules observed in the crystal asymmetric unit not loaded with the cofactor and trapped indeed in an open conformation analogous to the wild-type apo enzyme.

Overall models of mutant proteins D222A/Q223R and D222Q/Q223R are the best defined, spanning from A2 to V384 in both cases, while the wt holo enzyme as well as the D222S/Q223R are traceable in the electron density only till A375. Where the C-terminal fragment (375-384) is visible, it assumes a defined helical conformation, as in the case of the two mutant proteins D222A/Q223R and D222Q/Q223R, and plays an active role in shaping the active site region, binding to the $NADP^+$ cofactor, through direct interactions by Y382 CO (main chain) and the adenosine 5'-phosphate as well as mutated R223 (Figure 3C). The last is well defined in the electron density in both mutants, points toward the C-term helix and lays roughly parallel to the adenine moiety of $NADP^+$, defining stacking interactions with such aromatic electron density analogously to the wt Q223. In D222S/Q223R a major difference in the local arrangement surrounding adenosine 5'-phosphate of $NADP^+$ is accompanied by a relevant shift of such phosphate group (Figure 3B). As a consequence, R223 side chain is shifted away and gets poorly defined in the electron density, to give space to such rearrangement. A contribution due to cobalt ions (deriving from crystallization solutions, as noted above, see Figure S8), bound both where the C-term helix 375-384 is placed in the other mutant proteins and also close to H224, cannot be excluded in the case of D222S/Q223R, especially in the displacement of R223. However, metal cations do not enter in direct contact with the phosphate group and their presence is rather expected to favor ordered over flexible arrangements.

In all mutant proteins, the loop from 219 to 226 (where mutations have been introduced) experience a global moderate shift to accommodate the bulky $NADP^+$ cofactor. This is accompanied by an analogous adaptation of residues in between 258 and 262 shaping the top of cofactor binding cavity: such shift is slightly more pronounced in D222A/Q223R and D222Q/Q223R, while D222S/Q223R main chain maintains positions closer to the wt enzyme (Figure 3B).

D222 is mutated here into either serine, glutamine or alanine, serine being the most productive in terms of catalytic properties. All such substitutions imply the removal of a negative repulsive charge, still pointing their side chains toward the inner side in the active site. In particular, mutation to A222 results in reducing steric hindrance and preventing polar interactions, which could eventually leave the loop 219-226 even more free to adapt. Both Q and S 222 interact with the cofactor, even if glutamine directly contacts the adenosine 5'-phosphate while serine establishes hydrogen bonds through a water molecule bridging the interaction with the same 5'-phosphate. As expected, mutations 222-223

mainly impact on the loop they belong to (219-226). Indeed L226, F221 and H224 are shifted to enlarge the active site gate, more significantly in alanine and serine mutants then in glutamine one. Interestingly, the azide inhibitor, that occupies the internal formate binding site and is very well defined in all the structures presented here, experience a slight shift, that is minimal in the case of D222S/Q223R and progressively more evident in D222A/Q223R and D222Q/Q223R. This behavior - dictated by slight changes perturbing the overall active site - could justify the good affinity retained by the serine variant and worse performance of the others.

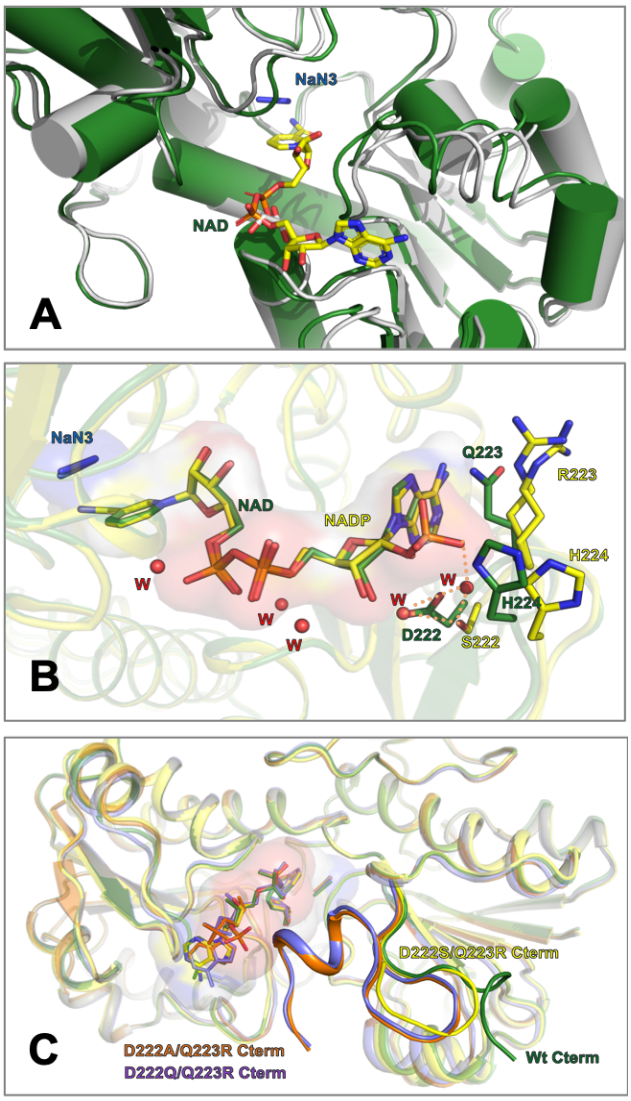

Figure 3. Cartoon representation of *Gra*FDH2 crystal structures: in panel **A** *Gra*FDH2 wt is shown in apo form (grey) and in complex with NAD^+ and NaN_3 (forest green); in panel **B** *Gra*FDH2 wt in complex with NAD^+ and NaN_3 (forest green) is compared to mutant D222S/Q223R structure in complex with $NADP^+$ and NaN_3 (yellow). Water molecules interacting with $NADP^+$ cofactor are shown as red spheres as well as those forming an hydrogen bonding network with Serine 222 and cofactor phosphate in the D222S/Q223R variant. Panel **C** shows a comparison of the C-terminus folding of wt *Gra*FDH2 holo structure and holo structures of variants.

Conclusions

Attempts to improve the catalytic efficiency of enzymes often encounter solubility and stability problems that account for huge limits in both screening and producing the best *in vitro* evolved variants. What protein engineering strategies generally struggle to consider, both at the computational and molecular level, are compensatory mutations that, instead, are rigorous determinants of Darwinian evolution. This work represents an example of how a synthetic biology project can tackle theorical engineering issues by examining practical results of natural evolution (at a very close point of view, in our case, *i.e.* two paralog genes). Indeed, the choice of changing the strategy proved successful: we shifted from the re-shaping of the low efficient, although naturally $NADP^+$-accepting, enzyme *Gra*FDH to the modification of the much more efficient, strictly NAD^+-dependent, *Gra*FDH2. The rational engineering of this latter enzyme, changing its cofactor specificity, permitted the obtaining of a new enzyme endowed with the sought characteristics. In particular, the *Gra*FDH2-D222S/Q223R variant retains a good affinity for formate, while acquiring $NADP^+$ specificity. Finally, concerning applicability, this work provides the biocatalysis community with a new NADPH regeneration enzyme, which is already among the best developed so far and, moving from the fine structural characterization here presented, might be further improved by next engineering.

Table 3. Kinetic parameters of the best reported $NADP^+$-dependent FDHs.

Enzyme	k_{cat} formate (s^{-1})	K_M formate (mM)	k_{cat} / K_M (M^{-1} s^{-1})	k_{cat} NADP+ (s^{-1})	K_M NADP+ (mM)	k_{cat} / K_M (M^{-1} s^{-1})	Reference
*Gra*FDH2 D222S/Q223R	3.53	23.66	1.50×10^2	3.08	0.14	2.26×10^4	This work
*Bd*FDH	4.39	5.66	7.80×10^2	4.04	1.17	3.45×10^3	[12]
*Lb*FDH	2.50	49.80	5.00×10^1	3.51	0.12	2.92×10^4	[8]
*Gra*FDH	6.11	191.25	3.00×10^1	3.96	0.85	4.66×10^3	[6]
*Myc*FDH-4M	n.r.	90.0	n.r.	3.08	0.14	2.10×10^4	[15]
*Myc*FDH-3M	n.r.	113.0	n.r.	7.90	1.10	8.58×10^3	[15]
*Bst*FDH	n.r.	55.50	n.r.	4.75	0.16	2.97×10^4	[10]
*Bsp*383FDH	6.12	126.79	5.00×10^1	2.77	0.79	3.00×10^1	[9]
*Bsp*184FDH	2.21	157	1.40×10^1	3.07	1.10	2.79×10^3	[9]
*Bac*FDH	n.r..	39.1	n.r.	1.07	3.50	3.10×10^2	[13]
*Cbo*FDH-D195Q/Y196R/Q197N	n.r.	n.r.	n.r.	0.79	0.03	2.72×10^4	[18]
*Lj*FDH	1.30	6.10	2.10×10^2	0.005	29.5	0.17	[11]
*Mut-Pse*FDH	n.r.	9.0	n.r.	2.50	0.15	1.67×10^4	[32]
*Sce*FDH D196A/Y197R	n.r.	1000	n.r.	0.13	7.60	2.10×10^1	[32]
*Cme*FDH D195S	n.r.	n.r.	n.r.	n.r.	n.r.	8.3	[33]

Values are shown for both formate oxidation with $NADP^+$ (on the left), and for $NADP^+$ (on the right). *Gra*: *Granulicella mallensis*, *Bd: Burkholderia dolosa* PC543, *Lb*: *Lactobacillus buchneri* NRRL B-30929, *Myc: Mycobacterium vaccae* N10, *Bst*: *Burkholderia stabilis*, *Bsp*383: *Burkholderia sp* 383, *Bsp184*: *Burkholderia sp* 184, *Bac*: *Bacillus sp.* F1, *Cbo*: *Candida boidinii, Lj: Lotus japonicus*, *Pse*: P*seudomonas sp.* 101, *Sce*: *Saccharomyces cerevisiae*, *Cme*: *Candida methylica*.
n.r. not reported

Experimental Section

Homology Modelling and analysis of electrostatic potentials

Structural superpositions were performed and viewed using UCSF Chimera v.1.12 (http://www.cgl.ucsf.edu/chimera/). Target protein sequence was modelled on the apo *Gra*FDH structure (4XYG) template using SWISS-MODEL (https://swissmodel.expasy.org/), without considering the 9 C-terminal amino acids modelled (since in 4XYG the last traceable residue was T377). Then, model structure was refined using SCWRL (http://proteinmodel.org/AS2TS/SCWRL/scwrl.html). Model quality was finally checked via the QMEAN server (https://swissmodel.expasy.org/qmean/). The resulting QMEAN6 Z-score for the *Gra*FDH2 homology model is - 0.80. After that, both *Gra*FDH structure and *Gra*FDH2 model were protonated with Chimera software. In order to perform analyses taking into account the influence of ionic strength (I), the spatial distribution of the electrostatic potential was calculated at both I = 0 M (Coulombic interactions unscreened by counter-ions) and I = 0.1 M (KH_2PO_4 phosphate buffer), assuming +3/-3 charges for the counter-ions. Prior to electrostatic potential calculations, partial charges and van der Waals radii were assigned with PDB2PQR considering a buffer pH of 7.5; then, linear Poisson Boltzmann (PB) equation calculations were carried out by using Adaptive PB Solver (APBS) through Opal web service.[34,35]

Gene cloning

The coding sequence of *Gra*FDH2 (NC_016631.1) was isolated from the genomic DNA of *Granulicella mallensis* MP5ACTX836, which was kindly furnished by Dr. S. Rawat (Department of Biochemistry and Microbiology, School of Environmental and Biological Sciences, The State University of New Jersey, USA). A first PCR using Xho_2_for and Nco_2_rev primers was performed to isolate the desired CDS and to insert two restriction sites: (1) a unique NcoI site at the natural ATG codon, meanwhile the natural stop codon was removed and in that position (2) a new XhoI site was introduced. An additional Overlap Extension PCR (OE-PCR) was performed in order to suppress an internal XhoI restriction site using XhoSup_2_for and XhoSup_2_rev primers The engineered *Gra*FDH2 variants (D222X/Q223X) were produced following the same protocol, except for different internal mutagenic primers (*Gra*FDH2_XX_for and *Gra*FDH2_XX_rev) (sequence of all primers are reported in Table S3). The final OE-PCR products were cloned into the pET28a(+) plasmid between the NcoI and XhoI restriction sites, thus producing pET28a-*Gra*FDH2 and pET28a-*Gra*FDH2-D222X/Q223X expression plasmids. The complete inserts sequencing was carried out using T7_for and T7_rev primers by BMR Genomics (Padua, Italy). All PCR amplifications were performed using the Phusion® High-fidelity DNA polymerase (NEB); restriction and

modification enzymes were also purchased by New England BioLabs (NEB, Ipswich, MA, USA).

Protein expression and purification

BL21 (DE3) *Escherichia coli* cells were transformed with pET28a-*Gra*FDH2 and plated onto LB agar plates supplemented with Kanamycin (50 μg ml^{-1}). Pre-cultures were carried out in LB medium (50 ml at 37 °C containing Kanamycin (50 μg ml^{-1}); larger cultures were grown in LB medium (800 ml) inoculated by overnight pre-culture (25 ml). Cells were grown in a shaking incubator at 37 °C to an optical density at 600 nm (OD600) of 0.4–0.6, then cells were induced by addition of isopropyl-β-D-1-thiogalactopyranoside (IPTG) up to 0.2 mM final concentration and cultivated at 16 °C overnight. Then, cells were harvested by centrifugation (4 °C, 10 minutes, 5000 g) and resuspended in KH_2PO_4 phosphate buffer (20 ml, pH 7.5, 0.1 M). Cell disruption was obtained by French Press (Constant Systems Cell Disruptor OneShot 1.35 kBar) and crude extract was centrifuged (4 °C, 30 minutes, 18000 g) to separate soluble and insoluble fractions. His-Select® Nickel Affinity resin (1 ml), previously equilibrated with phosphate buffer (pH 7.5, 0.1 M) was incubated for 30 minutes at 4 °C on a tube revolver with the soluble fraction. The loaded resin was then packed into an empty Poly-prep® column (10 ml) (Bio-Rad), washed by gravitational flow with five column volumes of phosphate buffer (pH 7.5, 0.1 M). Elution was performed by five column volumes of imidazole (0.25 M) in phosphate buffer (pH 7.5, 0.1 M). Eluted fractions (0.5 ml) were checked by 12 % SDS-PAGE in order to identify the fractions containing the desired protein and check their purity. Selected fractions (generally 3 to 6) were then pooled together and concentrated by ultrafiltration using Vivaspin concentrators (10 kDa cut-off). For crystallization studies, the buffer was exchanged with HEPES (pH 7.5, 0.05 M) using PD MidiTrap G-25 colums (GE Healthcare Life Sciences) following supplier protocol. The purified protein was quantified at the spectrophotometer (Agilent 8453), measuring its absorbance at 280 nm. The molar absorption coefficient was calculated using ProtParam Software (https://web.expasy.org/protparam/). The protein was finally stored at -20 °C upon addition of glycerol (20 % v/v). The same protocol described for *Gra*FDH2 wt was applied to *Gra*FDH2 protein variants.

Standard activity assay

Activity as formate dehydrogenase of the recombinant enzymes was demonstrated *in vitro* using the standard activity test reported in the previous work.[6] The standard assay (100 μL) was performed at 25 °C in KH_2PO_4 phosphate buffer (pH 7.5, 0.1 M) containing sodium formate (0.1 M), and nicotinamide cofactor (NAD^+ or $NADP^+$) (either 0.005 M or 0.02 M). Reactions were started through the addition of purified enzyme to a final concentration of 30 μg mL^{-1} and monitored for 60 seconds. The measurements were performed at least in duplicate. For the determination of the pH *optimum*, the standard assay (100 μL) was performed using sodium formate (0.1 M) and NAD^+ (0.02 M). Reactions were started by the addition of 30 μg mL^{-1} enzyme purified and measured over 60 seconds. In order to determine the specific activity (U mg^{-1}) of the enzyme.[36], a universal buffer with constant ionic strength was used: Tris-HCl (0.1 M), MES (0.05 M) and CH_3COOH (0.05 M) adjusted to the following pH values at 25 °C using 5 M NaOH or 5 M HCl: 4.0, 5.0, 6.0, 7.0, 8.0, 9.0, 10.0 and 12.0.

Determination of steady-state kinetic constants

Steady-state kinetic parameters K_M and k_{cat} were determined for the substrate formate and the accepted cofactors as reported.[6] Briefly, all reactions were started through the addition of purified enzyme to a final concentration of 30 μg mL^{-1} in the standard assay. All measurements were performed in duplicate. *Gra*FDH2 wt kinetics constants for the substrate formate were determined maintaining the concentration of NAD^+ constant (0.02 M), while varying sodium formate concentration in the range 0.0025 M to 0.5 M. For NAD^+ kinetic constants determination, the concentration of sodium formate was maintained constant (0.1 M), while cofactor concentration varied from 0.05 mM to 0.02 M. The kinetics constants for $NADP^+$ for the engineered *Gra*FDH2-D222X/Q223X variants were determined at 0,5 M sodium formate (0.2 M for D222S/Q223R), while cofactor concentration ranged from 0.05 mM to 0.02 M. Formate kinetic constants were measured in the presence of $NADP^+$ (0.005 M) by varying its concentration from 0.01 M to 0.75 M.

Size exclusion chromatography (SEC)

Molecular mass of native *Gra*FDH2 and its oligomeric state was determined by size exclusion chromatography. Superose™ 12 10/300 GL column was equilibrated with phosphate buffer (pH 7.0, 0.1 M). The flow rate for protein elution was 0.6 mL min^{-1}. Albumin from Rat Serum (RSA, MW 67 kDa) was used as reference standard.

Thermofluor assay

The apparent unfolding temperatures of the recombinant enzymes (T_m), in standard conditions (phosphate buffer, pH 7.5, 0.1 M) and in the presence of different co-solvents (ethanol, methanol, isopropanol, dimethyl sulfoxide and *tert*-butanol) present in different percentages (5 – 40 %), were determined using the Thermofluor method.[37] The effects of different pH on protein stability were also investigated using a Tris (0.1 M), MES (0.05 M), CH_3COOH (0.05 M) buffer system at three different pH values: 5.0, 7.0 and 9.0 (for details see pH activity assay). Briefly, the protein was opportunely diluted (down to 5 μM final concentration) in 25 μL of phosphate buffer (pH 7.5, 0.1 M) supplemented with different co-solvents and Sypro® Orange dye (Life Technologies) (5000X in DMSO, 3 μL) diluted 1/100. Thermal denaturation profile has been applied and monitored by StepOne Real-Time PCR System (Applied Biosystems) with 470 nm excitation filter and 570 nm emission filter. All experiments were performed in duplicate. A temperature gradient from 25 to 95 °C was applied (0.5 °C min^{-1}), and fluorescence data were recorded. A sigmoidal curve was obtained after plotting the fluorescence amount against the temperature. The T_m values were determined as the maximum of the derivative of the obtained sigmoidal curve using the software GraphPad Prism 6 (https://www.graphpad.com/scientific-software/prism/).

Crystallization, model building and refinement

Freshly purified recombinant proteins (20 mg mL^{-1} in HEPES pH 7.5, 0.05 M) were submitted to sparse matrix crystallization trials, applying the isothermal vapor diffusion method, partially automated by Oryx8 Robot (Douglas Instruments). All the JCSG-plus Screen conditions were screened using the sitting drop setup on MRC 96-well plates at 293 K. Drops were prepared by mixing equal volumes (0.3 μL) of mother liquor and of protein solution.
In order to obtain the holo form of the proteins, NAD^+ (0.01 M) and NaN_3 (0.005 M) (*Gra*FDH2 wt), or $NADP^+$ (0.01 M) and NaN_3 (0.005 M) (*Gra*FDH2-D222X/Q223X) were added to the enzyme preparation and co-crystallization was performed. For detailed crystal growth conditions see Supporting information file. Before data collection, crystals were either firstly soaked into a cryoprotectant solution (same precipitant agent supplemented with 20 % v/v PEG 3350 or 20 % glycerol) or directly frozen into liquid nitrogen. X-ray diffraction data were collected at 100 K at ESRF (Grenoble, France) synchrotron radiation source and Elettra (Trieste, Italy).

Diffraction data were processed and analyzed by the automated pipelines feasible at ESRF synchrotron. In particular, we used the data integrated and scaled by EDNA Autoprocessing framework (XDS, XSCALE, Pointless, Aimless).[38] Then, data were further cut to appropriate resolution by running aimless through the ccp4i2 suite.[39] The same interface was used in combination with Phenix suite[40] for any of the subsequent steps of phasing and refinement.

Briefly, *Gra*FDH2 structure was determined by molecular replacement (Phaser software)[41] using as template the model of *Gra*FDH2 built by Swiss Model as previously described (see Homology modelling). After few cycles of refinement, the most disordered regions and undefined loops were manually reconstructed with the support of Coot graphic interface.[42] The refinement steps were carried out by Refmac5[43] and Phenix software Refine[44].

Final model of apo enzyme (pdb 6T8C) was traced and fully visible from Ala2 to Ala375 for chain A and C and from Ala2 to Leu374 for chain B and D. The amino acids after Ala375 were poorly defined in the density maps and thus omitted. Final parameters obtained for the best dataset are summarized in Table S4.

Crystal structure of holo enzyme in complex with NAD^+ and NaN_3 (pdb 6T8J) were collected and processed analogously to the apo enzyme. Data were phased by molecular replacement using the *Gra*FDH2 apo structure as template. A clear electron density not attributable to protein chain was observed in the difference maps and allowed to define the binding and orientation of NAD^+ cofactor and azide inhibitor in the active site of the complex. Protein structure was clear and well defined from residue Ala2 to Gly371 in chain A, to Ala375 in chain B, to Gly372 in chain C and Asp370 in chain D, the last residues which were not defined in the density map were omitted.

Crystal structures of holo GraFDH2-D222X/Q223X (D222S/Q223R (pdb 6T6B), D222A/Q223R (pdb 6T9W), D222Q/Q223R (pdb 6T9X)) proteins in complex with $NADP^+$ and azide were collected and processed analogously to the wt FDH2.

Briefly, data were phased by molecular replacement (Phaser software)[41] using the protein model of the *Gra*FDH2 holo structure as template. Refinement was carried out analogously to wt enzyme. Experimental maps obtained in this manner were analyzed to detect the presence of $NADP^+$, azide and any other ligands due to the crystallization conditions. In particular, D222S/Q223R trapped three metal ions, two of them at the entrance of the active site cavity, and other metal coordinating moieties most likely caught from precipitation mixture (JCSG screen, Molecular Dimension). Details of space groups, quality of diffraction data as well as final refined models are given in Table S5 for all the structures solved and described here.

Acknowledgements

We thank Dr. Irene Righetto, Dr. Mattia Niero and and Oana Ilioaia for their technical assistance with bioinformatics tasks, enzymatic assays and *Chlamydomonas* manipulations, respectively. F. Z. and E. B. acknowledge financial support from *Agence Nationale de Recherche* (LabEx DYNAMO, ANR-11-LABX-0011-01) and *Fondazione Cassa di Risparmio di Padova e Rovigo* (*CARIPARO* Visiting Programme 2018/0559).

Keywords: biocatalysis • computational design • formate dehydrogenase • protein engineering • NADPH regeneration

[1] A. T. Martínez, F. J. Ruiz-Dueñas, S. Camarero, A. Serrano, D. Linde, H. Lund, J. Vind, M. Tovborg, O. M. Herold-Majumdar, M. Hofrichter, C. Liers, R. Ullrich, K. Scheibner, G. Sannia, A. Piscitelli, C. Pezzella, M. E. Sener, S. Kılıç, W. J. H. van Berkel, V. Guallar, M. F. Lucas, R. Zuhse, R. Ludwig, F. Hollmann, E. Fernández-Fueyo, E. Record, C. B. Faulds, M. Tortajada, I. Winckelmann, J.-A. Rasmussen, M. Gelo-Pujic, A. Gutiérrez, J. C. del Río, J. Rencoret, M. Alcalde, *Biotechnol. Adv.* **2017**, *35*, 815–831.

[2] F. Hollmann, I. W. C. E. Arends, D. Holtmann, *Green Chem.* **2011**, *13*, 2285–2314.

[3] A. M. Bezborodov, N. A. Zagustina, *Appl. Biochem. Microbiol.* **2016**, *52*, 237–249.

[4] H. Yamamoto and E. Carreira, in *Compr. Chirality*, **2012**, pp. 46–70.

[5] X. Wang, T. Saba, H. H. P. Yiu, R. F. Howe, J. A. Anderson, J. Shi, *Chem Cell Press* **2017**, *2*, 621–654.

[6] S. Fogal, E. Beneventi, L. Cendron, E. Bergantino, *Appl. Microbiol. Biotechnol.* **2015**, *99*, 9541–9554.

[7] A. S. Bommarius, M. Schwarm, K. Stingl, M. Kottenhahn, K. Huthmacher, K. Drauz, *Tetrahedron Asymmetry* **1995**, *6*, 2851–2888.

[8] S. Alpdağtaş, S. Yücel, H. A. Kapkaç, S. Liu, B. Binay, *Biotechnol. Lett.* **2018**, *40*, 1135–1147.

[9] B. Davis, A. Celik, G. Davies, K. Ruane **2013**, US 2013/0029378A1.

[10] R. Hatrongjit, K. Packdibamrung, *Enzyme Microb. Technol.* **2010**, *46*, 557–561.

[11] A. Andreadeli, E. Flemetakis, I. Axarli, M. Dimou, M. K. Udvardi, P. Katinakis, N. E. Labrou, *Biochim. Biophys. Acta* **2009**, *1794*, 976–984.

[12] S. Alpdağtaş, A. Celik, F. Ertan, B. Binay, *Eng. Life Sci.* **2018**, *18*, 893–903.

[13] H. T. Ding, D. F. Liu, Z. L. Li, Y. Q. Du, X. H. Xu, Y. H. Zhao, *J. Appl. Microbiol.* **2011**, *111*, 1075–1085.

[14] O. Carugo, P. Argos, *Proteins* **1997**, *28*, 10–28.

[15] K. Hoelsch, I. Sührer, M. Heusel, D. Weuster-Botz, *Appl. Microbiol. Biotechnol.* **2013**, *97*, 2473–2481.

[16] V. I. Tishkov, V. O. Popov, *Biomol. Eng.* **2006**, *23*, 89–110.

[17] A. Andreadeli, D. Platis, V. Tishkov, V. Popov, N. E. Labrou, *FEBS J.* **2008**, *275*, 3859–3869.

[18] W. Wu, D. Zhu, L. Hua, *J. Mol. Catal. B Enzym.* **2009**, *61*, 157–161.

[19] G. P. Özgün, E. B. Ordu, H. E. Tütüncü, E. Yelboğa, R. B. Sessions, N. Gül Karagüler, *Scientifica* **2016**, *2016*, 1–7.

[23] A. A. Alekseeva, V. V. Fedorchuk, S. A. Zarubina, E. G. Sadykhov, A. D. Matorin, S. S. Savin, V. I. Tishkov, *Acta Naturae* **2015**, *7*, 60-69.

[21] J. K. B. Cahn, C. A. Werlang, A. Baumschlager, S. Brinkmann-Chen, S. L. Mayo, F. H. Arnold, *ACS Synth. Biol.* **2017**, *6*, 326–333.

[22] J. Xiong, J. Minagawa, A. Crofts, Govindjee, *Biochim. Biophys. Acta BBA - Bioenerg.* **1998**, *1365*, 473–491.

[23] V. I. Tishkov, V. O. Popov, *Biochem. Biokhimiia* **2004**, *69*, 1252–1267.

[27] G. Kurt-Gür, E. Ordu, *3 Biotech* **2018**, *8*, 175-186.

[25] M. K. Mannisto, S. Rawat, V. Starovoytov, M. M. Haggblom, *Int. J. Syst. Evol. Microbiol.* **2012**, *62*, 2097–2106.

[26] E. G. Sadykhov, A. E. Serov, N. S. Voinova, S. V. Uglanova, A. S. Petrov, A. A. Alekseeva, S. Yu. Kleimenov, V. O. Popov, V. I. Tishkov, *Appl. Biochem. Microbiol.* **2006**, *42*, 236–240.

[35] V. O. Popov and V. I. Tishkov, in *Protein Struct. Kaleidosc. Struct. Prop. Funct.* **2003**, pp. 441-473.

[28] I. G. Shabalin, E. V. Filippova, K. M. Polyakov, E. G. Sadykhov, T. N. Safonova, T. V. Tikhonova, V. I. Tishkov, V. O. Popov, *Acta Crystallogr. D Biol. Crystallogr.* **2009**, *65*, 1315–1325.

[29] V. S. Lamzin, A. E. Aleshin, B. V. Strokopytov, M. G. Yukhnevich, V. O. Popov, E. H. Harutyunyan, K. S. Wilson, *Eur. J. Biochem.* **1992**, *206*, 441–452.

[30] Q. Guo, L. Gakhar, K. Wickersham, K. Francis, A. Vardi-Kilshtain, D. T. Major, C. M. Cheatum, A. Kohen, *Biochemistry* **2016**, *55*, 2760–2771.

[31] E. Krissinel, *J. Comput. Sci. Appl. Inf. Technol.* **2017**, *2*, 1–7.

[32] A. E. Serov, A. S. Popova, V. V. Fedorchuk, V. I. Tishkov, *Biochem. J.* **2002**, *367*, 841–847.

[33] N. Gul-Karaguler, R. B. Sessions, A. R. Clarke, J. J. Holbrook, *Biotechnol. Lett.* **2001**, *23*, 283–287.

[38] T. J. Dolinsky, J. E. Nielsen, J. A. McCammon, N. A. Baker, *Nucleic Acids*

Res. **2004**, *32*, 665–667.

[35] E. Jurrus, D. Engel, K. Star, K. Monson, J. Brandi, L. E. Felberg, D. H. Brookes, L. Wilson, J. Chen, K. Liles, M. Chun, P. Li, D. W. Gohara, T. Dolinsky, R. Konecny, D. R. Koes, J. E. Nielsen, T. Head-Gordon, W. Geng, R. Krasny, G.-W. Wei, M. J. Holst, J. A. McCammon, N. A. Baker, *Protein Sci.* **2018**, *27*, 112–128.

[36] H. A. Relyea, J. M. Vrtis, R. Woodyer, S. A. Rimkus, W. A. van der Donk, *Biochemistry* **2005**, *44*, 6640–6649.

[37] M. W. Pantoliano, E. C. Petrella, J. D. Kwasnoski, V. S. Lobanov, J. Myslik, E. Graf, T. Carver, E. Asel, B. A. Springer, P. Lane, F. R. Salemme, *J. Biomol. Screen.* **2001**, *6*, 429–440.

[38] W. Kabsch, *Acta Crystallogr. D Biol. Crystallogr.* **2010**, *66*, 125–132.

[39] M. D. Winn, C. C. Ballard, K. D. Cowtan, E. J. Dodson, P. Emsley, P. R. Evans, R. M. Keegan, E. B. Krissinel, A. G. W. Leslie, A. McCoy, S. J. McNicholas, G. N. Murshudov, N. S. Pannu, E. A. Potterton, H. R. Powell, R. J. Read, A. Vagin, K. S. Wilson, *Acta Crystallogr. D Biol. Crystallogr.* **2011**, *67*, 235–242.

[40] P. D. Adams, P. V. Afonine, G. Bunkóczi, V. B. Chen, I. W. Davis, N. Echols, J. J. Headd, L.-W. Hung, G. J. Kapral, R. W. Grosse-Kunstleve, A. J. McCoy, N. W. Moriarty, R. Oeffner, R. J. Read, D. C. Richardson, J. S. Richardson, T. C. Terwilliger, P. H. Zwart, *Acta Crystallogr. D Biol. Crystallogr.* **2010**, *66*, 213–221.

[41] A. J. McCoy, R. W. Grosse-Kunstleve, P. D. Adams, M. D. Winn, L. C. Storoni, R. J. Read, *J. Appl. Crystallogr.* **2007**, *40*, 658–674.

[42] P. Emsley, K. Cowtan, *Acta Crystallogr. D Biol. Crystallogr.* **2004**, *60*, 2126–2132.

[43] G. N. Murshudov, P. Skubák, A. A. Lebedev, N. S. Pannu, R. A. Steiner, R. A. Nicholls, M. D. Winn, F. Long, A. A. Vagin, *Acta Crystallogr. D Biol. Crystallogr.* **2011**, *67*, 355–367.

[44] P. V. Afonine, R. W. Grosse-Kunstleve, N. Echols, J. J. Headd, N. W. Moriarty, M. Mustyakimov, T. C. Terwilliger, A. Urzhumtsev, P. H. Zwart, P. D. Adams, *Acta Crystallogr. D Biol. Crystallogr.* **2012**, *68*, 352–367.

10.1002/cctc.201902089

WILEY-VCH

FULL PAPER

The race towards NADP$^+$-specificity: a new FDH was identified and successfully engineered in order to switch its cofactor specificity.

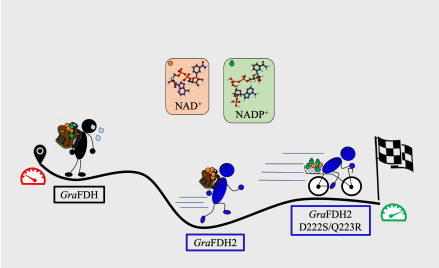

Marina S. Robescu, Rudy Rubini, Elisa Beneventi, Michele Tavanti, Chiara Lonigro, Francesca Zito, Francesco Filippini, Laura Cendron and Elisabetta Bergantino**

Page No. – Page No.

From the Amelioration of a NADP$^+$-dependent Formate Dehydrogenase to the Discovery of a New Enzyme: Round Trip from Theory to Practice